ResearchGate

See discussions, stats, and author profiles for this publication at: http://www.researchgate.net/publication/241076339

Monitoring snow cover variability in an agropastoral area in the Trans Himalayan region of Nepal using MODIS data with improved cloud removal methodology

ARTICLE *in* REMOTE SENSING OF ENVIRONMENT · MAY 2011

Impact Factor: 6.39 · DOI: 10.1016/j.rse.2011.01.006

CITATIONS

17

2 AUTHORS, INCLUDING:

Peter Andersen

University of Bergen

12 PUBLICATIONS **61** CITATIONS

SEE PROFILE

Available from: Peter Andersen

Retrieved on: 31 August 2015

Remote Sensing of Environment 115 (2011) 1234–1246

Contents lists available at ScienceDirect

Remote Sensing of Environment

journal homepage: www.elsevier.com/locate/rse

Monitoring snow cover variability in an agropastoral area in the Trans Himalayan region of Nepal using MODIS data with improved cloud removal methodology

Keshav Prasad Paudel *, Peter Andersen

Department of Geography, University of Bergen, Fosswinkelsgate 6. N-5007, Bergen, Norway

ARTICLE INFO

Article history:
Received 18 October 2010
Received in revised form 10 January 2011
Accepted 13 January 2011

Keywords:
MODIS snow data
Cloud removal method
Zonal snowline
Zonal snow cycle
Snow cover variability
Himalaya
Cryosphere

ABSTRACT

Monitoring the extent and pattern of snow cover in the dry, high altitude, Trans Himalayan region (THR) is significant to understand the local and regional impact of ongoing climate change and variability. The freely available Moderate Resolution Imaging Spectroradiometer (MODIS) snow cover images, with 500 m spatial and daily temporal resolution, can provide a basis for regional snow cover mapping, monitoring and hydrological modelling. However, high cloud obscuration remains the main limitation. In this study, we propose a five successive step approach — combining data from the Terra and Aqua satellites; adjacent temporal deduction; spatial filtering based on orthogonal neighbouring pixels; spatial filtering based on a zonal snowline approach; and temporal filtering based on zonal snow cycle — to remove cloud obscuration from MODIS daily snow products. This study also examines the spatial and temporal variability of snow cover in the THR of Nepal in the last decade. Since no ground stations measuring snow data are available in the region, the performance of the proposed methodology is evaluated by comparing the original MODIS snow cover data with least cloud cover against cloud-generated MODIS snow cover data, filled by clouds of another densely cloud-covered product. The analysis indicates that the proposed five-step method is efficient in cloud reduction (with average accuracy of >91%). The results show very high interannual and intra-seasonal variability of average snow cover, maximum snow extent and snow cover duration over the last decade. The peak snow period has been delayed by about 6.7 days per year and the main agropastoral production areas of the region were found to experience a significant decline in snow cover duration during the last decade.

© 2011 Elsevier Inc. All rights reserved.

1. Introduction

Snow and ice cover play an important role within the global heat budget (Bates et al., 2008; Berry, 1981; Lemke et al., 2007; Robock, 1980). Its variation in space and time is the result of variability in earth's climate system, as well as being one of the important controlling parameters for global to regional climate variability (Barnett et al., 1989). Moreover, the extent and dynamics of snow and ice cover affect many hydrological, physical, chemical and biological processes (Robinson et al., 1993). Thus, change and variability in the Himalayan cryosphere, popularly referred to as 'the water tower of Asia', have significant local, downstream and global feedback effects (Erikson et al., 2009). In popular environmental narratives, the main focus has been on retreating glaciers, while snow cover has received less attention. In the high altitude snow/glacier fed basins of the Himalayan region (Singh & Bengtsson, 2005), the local agropastoral production relies heavily on snow cover dynamics. Thus, information of spatial and temporal pattern of snow/ice cover in the region is important for a wide variety of scientific studies, management applications and the sustainable development of the region.

The Himalayan region of Nepal is considered to be one of the most critical regions in terms of global warming. Studies indicate that the warming rate in the region has been 0.06 °C to 0.12 °C per year, much greater than global average of 0.74 °C over the last 100 years (Shrestha et al., 1999; Solomon et al., 2007), and it has increased progressively with elevation (Liu & Chen, 2000; Shrestha et al., 1999). As a result, the Himalayan region has experienced the highest glacial retreat in the world (Cruz et al., 2007; Dyurgerov et al., 2005) and the greatest decline in snow cover and ice mass. However, there is a substantial data and knowledge gap concerning the snow cover dynamics in the region (Erikson et al., 2009; Messerli et al., 2004; Xu et al., 2009).

There are no snow-monitoring observation stations in the Nepalese Himalaya. Mapping and monitoring the snow cover with field measurements is costly and almost impossible for large catchments. The freely available Moderate Resolution Imaging Spectroradiometer (MODIS) snow cover products (Hall et al., 2002), with 500 m spatial and daily temporal resolution, can provide a basis for regional snow-cover mapping, monitoring and hydrological modelling (Liang et al., 2008; Tekeli et al., 2005). The accuracy of MODIS snow-cover data, under clear sky conditions has been tested by researchers in different parts of the world and shows a very high

* Corresponding author. Tel.: +47 98683685; fax: +47 55583099.
E-mail addresses: keshav.paudel@geog.uib.no, keshav.paudel@gmail.com (K.P. Paudel).

0034-4257/$ – see front matter © 2011 Elsevier Inc. All rights reserved.
doi:10.1016/j.rse.2011.01.006

agreement (overall agreement of >93%) (cf. Hall & Riggs, 2007; Hall et al., 1998; Liang et al., 2008; Maurer et al., 2003; Parajka & Blöschl, 2006; Wang et al., 2008; Zhou et al., 2005). However, high cloud obscuration in MODIS snow-cover data is the main limitation in many applications. Several methods have been developed to reduce the cloud cover pixels from MODIS products. They include one or a combination of different approaches, such as combining Terra and Aqua MODIS data, spatial filtering, temporal filtering, eight days' maximum snow-cover extent, and time series of thresholds of snow accumulation and melt. Considering the local crossing time difference between the Terra and Aqua satellites, most of the studies implemented the combination of both MODIS products successfully, to reduce cloud cover (Gafurov & Bárdossy, 2009; Parajka & Blöschl, 2008; Wang et al., 2009), since it is possible to have different cloud coverage within a difference of three hours (as local equatorial crossing time of Terra is 10:30 a.m. in a descending node, and of Aqua is 1:30 p.m. in ascending node). The spatial filter based on neighbouring 4 or 8 pixels is another procedure (Gafurov & Bárdossy, 2009; Parajka & Blöschl, 2008; Tong et al., 2009; Xie et al., 2009). However, there is the possibility of sacrificing some of the spatial resolution by replacing cloud pixels with the majority class of neighbouring pixels (Gao et al., 2010). Instead, spatial filtering based on only orthogonal neighbouring pixels can maintain better spatial resolution; for example, Gafurov and Bárdossy (2009) found very low level error using this procedure.

Fixed day or flexible composite maximum snow-cover product, which is produced by compositing the daily images of the predefined temporal window, is used as a temporal approach to maximize the number of snow pixels while minimizing the number of cloud pixels (Gao et al., 2010; Liang et al., 2008; Parajka & Blöschl, 2008; Riggs et al., 2006; Xie et al., 2009). The MODIS 8-day Snow Cover Products, MOD10A2 and MYD10A2, which combine two to eight days of the snow-cover products, are the representatives of such a fixed-day combination. These approaches can largely reduce the cloud cover, but minimize the temporal resolution. Temporal filtering as the direct replacement of cloud pixel, by the most recent preceding non-cloud observations at the same pixel, is another commonly used temporal approach (Parajka & Blöschl, 2008; Zhao & Fernandes, 2009). However, without incorporating the snowfall accumulation (expansion of snow cover) and ablation period in such fixed-day combinations, there is a risk of losing temporal resolution. Recently, some studies have shown that temporal deduction using the information from preceding and following days on the same pixel can remove the cloud, while preserving temporal resolution (cf. Gafurov & Bárdossy, 2009; Gao et al., 2010). Gafurov & Bárdossy's threshold day of snow-accumulation start and complete melt is based on time series information per pixel, and attempts to reclassify cloud pixels to snow or land, according to their relative position to the seasonal cycle of snow accumulation and ablation. However, their method assumes only one snow cycle, that is continuous days of snow cover from first snow appearance (accumulation start) day to complete snowmelt day, in a given pixel in a year. This does not fully represent the multi-snow cycle pattern within a year, which is the most common pattern in the drier THR, and thus their method ignores the intraseasonal variability of snowmelt and accumulation.

In mountain regions, slope, aspect and elevation affect the snow accumulation and snowmelt owing to the lapse rate of temperature, energy balance and windward/leeward effects. Incorporation of these topographic effects can further improve the cloud removal approaches. Recently, Parajka et al. (2010) have developed a snowline approach, reclassifying pixels assigned as clouds to snow or land, according to their relative position to the regional snowline elevation. Similarly, Gafurov and Bárdossy (2009) have also incorporated elevation in spatial filtering based on eight neighbouring pixels, as well as in their snow transition elevation approach. However, they have not considered the illumination and shadowing effects as the function of topography. Thus, considering the effects of aspect, the zonal (sub-basin further divided in to local landscape unit based on aspect and land cover) snowline can truly represent the topographic effect on snow accumulation and melting rather than the assumed regional 'snow transition line'.

This paper aims to remove cloud obscuration from snow cover data and improve some current cloud-reducing approaches, based on a five successive steps approach, combining data from the Terra and Aqua satellites, adjacent temporal deduction, spatial filtering based on orthogonal neighbouring pixels, spatial filtering based on zonal snowline, and temporal filtering based on the pattern of snow accumulation and melting. Subsequently, this study also examines the spatial and temporal variability of snow cover in the THR of Nepal during the last decade.

2. Study area

The Trans Himalayan region, in the rain shadow of the great Himalaya, lies between the Himalayan range and the Tibetan plateau. The study area, located approximately between 28°25′ to 29°20′N and 83°25′ to 84°35′ E, covers two Trans Himalayan districts of Nepal, Mustang and Manang (Fig. 1). The total land area is 5819 km^2 with the elevation ranging from about 1830 m to 8167 m above sea level (asl). Topographically, 96% of the area lies in the elevation zone above 3000 m asl, with 43% of the area above 5000 m asl. Rangeland is the dominant land resource covering 42.1%, followed by forest (4.5%) and cultivated land (1.3%). The valley floor of Lower Mustang and Lower Manang, at altitudes below 3000 m asl, is characterized by a cold temperate climate with mean annual precipitation of 880 mm. The elevation zone 3000 to 5000 m asl has an alpine semi-arid to arid climate with mean annual precipitation of 220 mm and tundra climate above ca. 5000 m asl. Upper Mustang is the driest region, and has 164 mm average annual precipitation with 35% coefficient of variation between 1973 and 2008. In the lower parts, most of the precipitation occurs during the monsoon (Jun–Sep) as rainfall, and during the winter (Dec–Feb) as snowfall. At very high altitude, all precipitation occurs in the form of snow, and the main snowfall is assumed to fall during the monsoon. Mean maximum/minimum temperatures in 1950–2007 in the study area were 20.9/11.3 in the monsoon months, 15.9/4.3 in the post-monsoon period (Oct–Nov), 17.7/4.5 in the pre-monsoon months (Mar–May) and 11.2/−1.2 in the winter. The maximum temperature recorded in Mustang is 25.9 °C and in Manang 24.5 °C and, according to the records, temperature freezes to as low as −20 °C in Mustang and −12.4 °C in Manang. Strong winds and intense sunlight are the common climatic features in both Manang and Mustang districts. The study area is the head-water environment of the Marshyangdi and Kali Gandaki Rivers. Both are tributaries to the Gandaki (also known as Narayani, Gandak) River, one of the major rivers of Nepal and the tributary to the Ganges River.

Agropastoral production is the primary source of livelihood for the area. In the arid/semi-arid areas, cultivation is primarily dependent on snowmelt and, to a lesser extent, on glacier fed irrigation. Non-irrigated fields depend on moisture from in situ snowmelt and precipitation including runoff from snowmelt/precipitation from the local catchments. The significant role of snow cover duration and pattern in rangeland production in high land pastures of the region as perceived by local people, has been discussed elsewhere (Paudel, 2006; Paudel & Andersen, 2010).

3. Methods

3.1. Data

MODIS is an optical instrument installed on the Terra and Aqua satellites of the NASA Earth observation system. It uses a cross-track scanner and acquires the imagery of the earth's surface and cloud

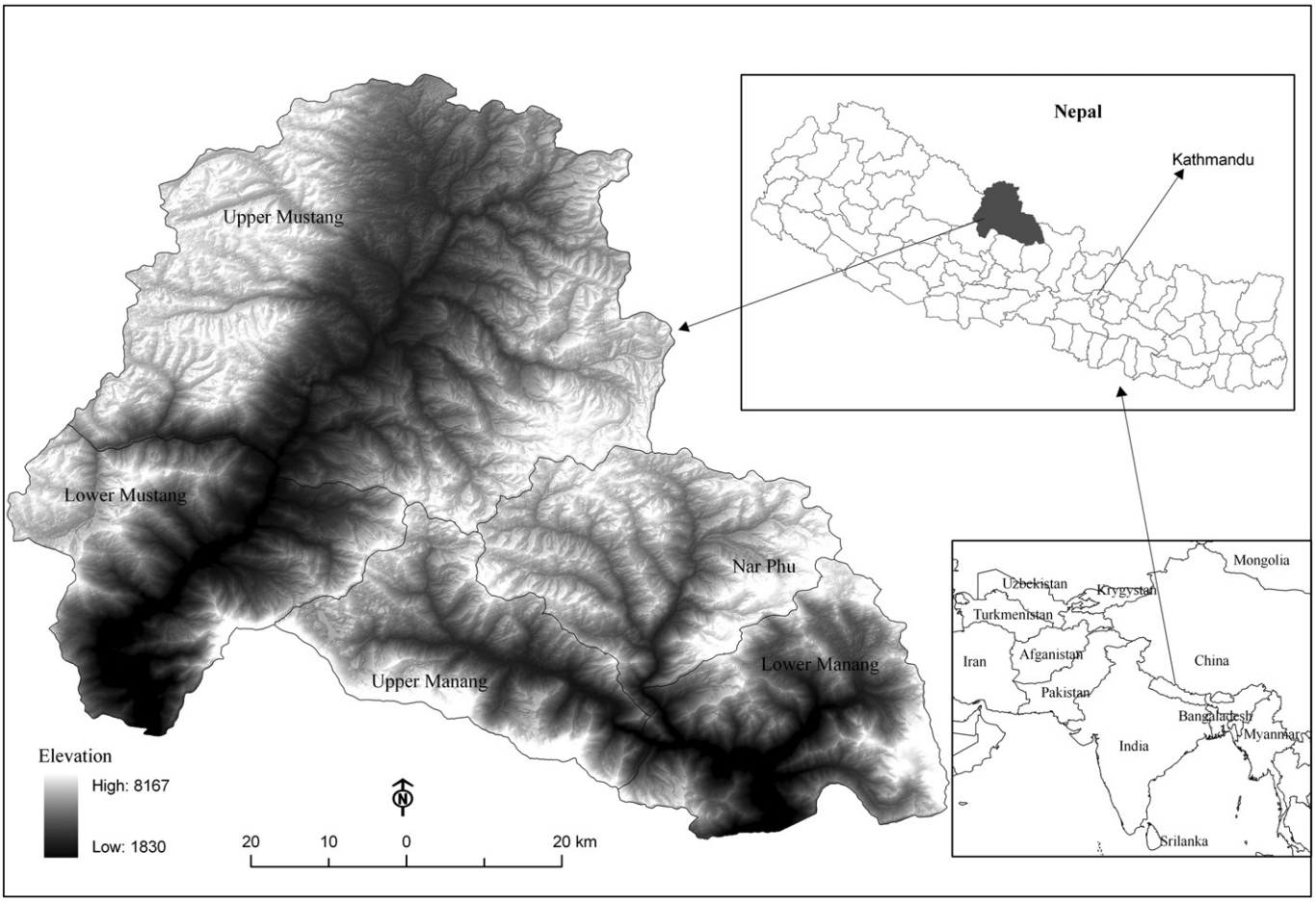

Fig. 1. Location of the study area: Upper Mustang and Lower Mustang lie in Mustang district and Nar Phu; Lower Manang and Lower Manang region lie in Manang district.

through a set of 36 discrete spectral bands, covering the visible and thermal infrared parts of electromagnetic spectrum, from about 0.4 to 14.0 μm (cf. Barnes et al., 2002; Guenther et al., 2002; Hall et al., 1995; Hall et al., 2002). The spatial resolution at the nadir of the MODIS sensor varies, and ranges from 250 m to 1 km, with spectral band. The first MODIS satellite Terra was launched in December 1999 and started to deliver data in February 2000, and the second Aqua satellite was launched in May 2002. Both Terra and Aqua have a sun-synchronous, near-polar, circular orbit. The MODIS snow product is based on the normalized difference snow index (NDSI) and set of thresholds and decision rules (cf. Hall et al., 2001; Hall et al., 2002; Riggs et al., 2006; Salomonson & Appel, 2004). Generally, November to March is considered to be the snow season in the rangelands of the region. However, considering some events of early and late snowfall, as evidenced from local oral history, we selected October to April as the snow season (window of analysis) in this study. All the available MODIS daily snow cover products, MOD10A1 and MYD10A1 (MODIS Terra/Aqua Snow Cover Daily L3 Global 500 m SIN GRID V005), for the period 1 October to 30 April, 2000–2010, were used in this study (Table 1). However, since the Aqua satellite started to deliver snow cover data from July 2002, we only used Terra snow cover daily data for the period 2000–2002. The study area lies within the MODIS tile H25V06. The MODIS Reprojection Tool (MRT, 2008) was used to project MODIS images into Universal Transverse Mercator (UTM) projection and to convert to GEOTIFF.

The MODIS snow cover image has six observed land cover characteristics that include snow, no snow (or land), lake, ocean, snow-covered water body (lake ice), cloud and five missing, unusable data or other condition classes that include missing sensor data, no decision, night (darkness, terminator or polar), saturated MODIS sensor detector, and fill (no data expected for pixel). In the total MODIS recorded data, the classes *missing*, *no decision* and *saturated* were less than 0.8%, while the *fill* class were 2.4% and 3.5%, respectively, for Terra and Aqua images in the study area. The occurrence of fill and other unusable pixel data was sporadic temporally and spatially through the study period, so replacing such filled or unusable pixel data with good observation is a reasonable approach to handling that data. So during the cloud removal processing, these were treated as 'cloud'. We reclassified snow cover images into three categories: that is, original *snow* and *lake ice* classes into 'snow' category; *no snow* and *lake* classes into 'no snow' category; and *cloud* and all other missing/unusable classes into 'cloud' category. In the algorithm used in this paper, snow, no snow and cloud were coded as 200, 25 and 1, respectively. After reclassification, 52.3% of the available Terra images and 72.7% Aqua images had a cloud cover larger than 10%.

The NASA Shuttle Radar Topographic Mission (SRTM) digital elevation model (DEM) data with 90 m spatial resolution was obtained from the CGIAR Consortium for Spatial Information (CGIAR-CSI) (http://srtm.csi.cgiar.org). The resolution of DEM was resampled to match the 500 m spatial resolution of snow-cover data. An aspect and slope map of the study area was derived from the DEM. Additionally, a land-cover map generated in 2000 by the Survey Department, Nepal Government, was obtained and updated with a land-cover map prepared by the authors using supervised classification method from SPOT 4 (XI), 20 m resolution images (16 Oct, 2008).

3.2. Cloud removal methodology

We propose a set of five steps, based on a combination of different spatial and temporal information, to reduce cloud obscuration from

Table 1
MODIS snow cover images used in this study.

Snow season	Terra (MOD10A1) images								Aqua (MYD10A1) images							
	Total images	Missing date	Mean cloud (%)	Frequency (%) of images with cloud cover larger than					Total images	Missing date	Mean cloud (%)	Frequency (%) of images with cloud cover larger than				
				10%	25%	50%	75%	90%				10%	25%	50%	75%	90%
1 Oct 00–30 Apr 01	211	27 Oct 00	23.9	48.8	32.2	17.1	9.5	6.2	–	–	–	–	–	–	–	–
1 Oct 01–30 Apr 02	201	6 Nov 01, 20–28 Mar 02, 15 Apr 02	26.14	47.3	27.9	15.9	8.0	5.0	–	–	–	–	–	–	–	–
1 Oct 02–30 Apr 03	211	1 Feb 03	25.99	57.3	35.1	17.5	10.4	5.7	212		36.87	74.5	52.4	30.7	16.5	11.8
1 Oct 03–30 Apr 04	204	17–24 Dec 03, 19 Feb 04	24.03	49.5	32.8	19.6	9.3	5.9	213		34.72	67.9	48.1	31.1	13.7	7.5
1 Oct 04–30 Apr 05	212		36.78	61.6	47.9	30.8	22.7	14.7	212		47.96	77.4	63.7	44.8	31.1	20.8
1 Oct 05–10 May 06	222		25.08	50.7	31.8	21.3	11.4	6.2	222		41.63	69.8	48.1	32.1	17.5	9.0
1 Oct 06–30 Apr 07	212		26.35	54.3	36.2	21.0	10.0	5.2	212		39.61	75.9	57.1	33.5	20.3	10.8
1 Oct 07–30 Apr 08	213		26.82	57.6	37.1	20.5	10.5	7.1	212	21 Dec 7	36.99	78.3	50.5	31.1	18.4	9.4
1 Oct 08–30 Apr 09	208	20–23 Dec 08	19.59	45.7	29.8	10.1	4.8	2.9	212		31.85	67.5	48.1	26.4	12.3	4.7
1 Oct 09–30 Apr 10	211	6 Mar 10	26.01	50.2	32.5	14.8	9.6	5.3	212		35.06	70.6	50.2	31.3	14.7	10.0
Total	2105	27							1707	1						

MODIS snow-cover images. Each step, explained in the following subsections (from 3.2.1 to 3.2.5), was performed in sequence and the output from each step was the input for the next step. The analysis was done in Arc GIS using the Python programming language.

3.2.1. Terra–Aqua snow-cover image composites

The first step combines observations (from Terra and Aqua) on the same day with about three hours time difference. The compositing rules are similar to the MOD10A2 generation algorithm and are based on the following prioritization scheme: snow – no snow – cloud (Gao et al., 2010; Xie et al., 2009). If snow cover was found in any satellite image pairs, the pixel was assigned as snow. If the pixel was observed as 'no snow' by one satellite and cloud by another, the cell is assigned as 'no snow' as true pixel cover. Since the assigned code integers of snow (200), no snow (25) and cloud (1) are in decreasing order, the maximum function was used to compute Terra–Aqua snow cover image composite as:

$$S_{(y,x,t)} = \max\left(S^{T}_{(y,x,t)},\ S^{A}_{(y,x,t)}\right) \quad (1)$$

where, y and x are the indices for row and column, and t is the index for day of pixel S. S^T and S^A denote Terra and Aqua pixels respectively.

In the case of missing observation by one satellite on any day (Terra or Aqua), the product of the other is used directly as the output of the first step. For the period 2000–2002 when only Terra data was available, the original Terra data is used directly as the output of the first step.

3.2.2. Adjacent temporal deduction

This step deduces the surface condition of cloud-covered pixel based on the one day forward and one day backward information of same pixel (Gao et al., 2010). It is based on the assumption that if both the previous and the next day of the cloud pixel have the same surface condition (either snow or no snow), the surface cover stayed constant in cloudy weather conditions (Gafurov & Bárdossy, 2009). Hence, if the corresponding pixel of both the previous and the next day of observed day are snow, the cloud cover pixel ($S^{c}_{(y,x,t)}$) is set as snow (Eq. (2)). Similarly, a cloud pixel is deduced as no snow if the corresponding pixel of both the previous and the next day has 'no snow' cover (Eq. (3)). In other conditions, the cloud pixel remains as cloud.

$$\text{if } \left(S_{(y,x,t-1)} = 200 \text{ and } S_{(y,x,t+1)} = 200\right),\ S^{c}_{(y,x,t)} = 200, \quad (2)$$

$$\text{if } \left(S_{(y,x,t-1)} = 25 \text{ and } S_{(y,x,t+1)} = 25\right),\ S^{c}_{(y,x,t)} = 25 \quad (3)$$

3.2.3. Spatial filtering based on orthogonal neighbouring pixels

This approach assigns the cloud covered pixel as 'snow' if the majority of its orthogonal neighbours are 'snow' covered. Similarly, cloud pixel is set as 'no snow' when at least three out of its four direct neighbour pixels are of the 'no snow' class.

3.2.4. Zonal snow transition line approach

Previous studies have shown that snowfall and snow-cover distribution and depletion pattern in mountainous regions are largely influenced by topography, basin orientation and land-cover classes (cf. Baral & Gupta, 1997; Mitchell & DeWalle, 1998; Seyfried & Wilcox, 1995). Thus, we can assume that in a given zone, a landscape unit within a sub-basin further subdivided by a combination of aspect and land-cover classes, snow at a higher elevation accumulates earlier and melts later than at a lower elevation, owing to the lapse rate of temperature and energy balance. Hence, based on relative altitudinal characteristics of snow and no snow cover pixels, it is possible to deduce snow transition elevation for a day in a given zone. The concept is to find the elevation of lowest snow-cover pixel and the snowline of the day, above which there is continuous snow cover. The effectiveness of this approach depends upon two factors. First, on the precise delineation of zone; that is, the effect of basin orientation, land-cover class and topographic factors other than elevation on snow-cover distribution and depletion should be homogenous in all pixels in a zone. Second, on the amount of the cloud free pixels in the given zone resulting from the previous three steps. We first divided the study area into sub-basins based on the DEM and drainage map. Subsequently, we subdivided all sub-basins by major aspect classes (north, south, east and west) and land-cover classes (vegetation cover and bare rock), amounting to 316 zones in total (Fig. 2a). In order to make sure that snow-covered pixels were correctly reclassified, at least 25% cloud-free pixel was used as the minimum threshold of cloud-free in a given zone.

In this study, the snowline threshold for a given zone was defined as the minimum snow-cover elevation if that elevation was greater than the maximum elevation of no snow cover pixels. Based on this, all cloud pixels above the snowline threshold were assigned as snow (Eq. (4)). However, when this condition was not met (in this study, we found only 4.3% cases where this assumption was not met), we defined the snowline threshold as the zonal mean of snow-cover pixels (Eq. (5)), similar to Parajka et al. (2010)'s regional snowline. In our case it was computed for the zone, not for the whole study area. At this point we considered that snow cover could be absent or sporadic on very steep slopes (slope>60°) (Guglielmin et al., 2003). Similarly, the elevation of cloud pixel of the given zone was compared with the zonal mean elevation of no snow cover pixels (zonalmean (H_z^{NS})) and the zonal minimum elevation of snow cover pixel. Subsequently, it

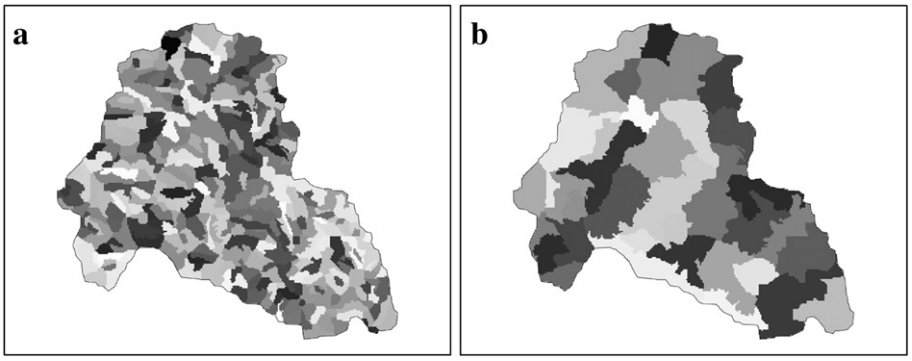

Fig. 2. Zone used for: a) zonal snow transition approach; and b) zonal snow cycle step.

was assigned no snow cover if it was lower than both of them (Eq. (6)).

$$\text{if } \left(H^{c}_{(y,x)} > \text{zonalmin}\left(H^{S}_{z}\right) > \text{zonalmax}\left(H^{NS}_{z}\right) \text{ and } C_z < 75 \text{ and } S < 60\right), S^{c}_{(y,x,t)} = 200 \quad (4)$$

$$\text{if } \left(H^{c}_{(y,x)} > \text{zonalmean}\left(H^{S}_{z}\right) > \text{zonalmax}\left(H^{NS}_{z}\right) \text{ and } C_z < 75 \text{ and } S < 60\right), S^{c}_{(y,x,t)} = 200 \quad (5)$$

$$\text{if } \left(H^{c}_{(y,x)} < \text{zonalmean}\left(H^{NS}_{z}\right) < \text{zonalmin}\left(H^{S}_{z}\right) \text{ and } C_z < 75\right), S^{c}_{(y,x,t)} = 25 \quad (6)$$

where, $S^{c}_{(y,x,t)}$ is the cloud cover pixel and $H^{c}_{(y,x)}$ is the elevation of that pixel. zonalmin(H^{S}_{z}), zonalmean(H^{S}_{z}) and zonalmax(H^{NS}_{z}) are the minimum elevation of all snow-covered pixels, the mean elevation of all snow pixels and the maximum elevation of all 'no snow' class pixels in the given zone, respectively. C_z is the percentage of cloud cover in the given zone and S is the slope of the pixel in degrees.

3.2.5. Zonal snow cycle

This step is based on a time series analysis of snow cycle(s) — accumulation and melt pattern — of each 'snow zone' over the snow season. Snow zone (SZ) in this step is considered as the homogenous unit in terms of snow cycle that is having similar pattern of snow occurrence (snow accumulation and melt). In zones delineated in step four, a group of adjacent zones can have a similar snow cycle pattern. In order to derive effective and feasible numbers of SZ, we merged adjacent zones which showed homogenous patterns of snow cycle in the last ten years, based on correlation analysis. We first computed total snow cover for each day in a zone from the output of step four. Adjacent zones having a correlation greater than 0.8 in terms of snow-cover duration in the last 10 years were merged. As a result, 36 SZ were derived altogether (Fig. 2b), and used for further analysis.

A snow cycle of a given SZ is defined as the period from the snow accumulation start day (D^{s}_{a}) to the minimum snow extent day (D^{s}_{min}), the day before the next D^{s}_{a}, is considered as a snow cycle of the given SZ (Fig. 3a). Snow accumulates either in a single day or over a few continuous days of snowfall. The maximum snow cover extent day (D^{s}_{max}) of the given SZ in this study is defined as the day of snowfall in the former case and the last day of the snowfall in the latter case, in a snow cycle. In the case of single effective snowfall, both D^{s}_{a} and D^{s}_{max} will be the same. In order to identify threshold days of D^{s}_{a}, D^{s}_{max} and D^{s}_{min} of each snow cycle, we first plotted the graph of the time series of total snow cover area against Julian days for each snow zone, for each snow season (for instance, see Fig. 3b). From the visual inspection of the graph and comparing it with the cloud percentage of the day in the given SZ, we identified threshold days of the cycle. The fluctuation of snow cover equal to, or smaller than, the cloud percentage of the given day in the given SZ were considered as the fluctuation owing to cloud, so only larger fluctuations (greater than cloud percentage) were considered to identify snow cycles. Based on the temporal position of cloud pixel in a snow cycle, the following rules were employed to reclassify the cloud pixel as 'snow' or 'no snow':

(a) If the pixel has 'no snow' cover on the maximum snow cover extent day (it may happen for lower elevation pixel if there is snowfall only in higher elevation in the given zone) and the cloud in following days, the cloud pixels are reclassified as 'no snow cover' till D^{s}_{min}.
(b) In the time series from D^{s}_{min} to D^{s}_{max} of a snow cycle, if the pixel has 'snow' on the day t and cloud in the preceding days (t − 1 …t − n), the pixel of the preceding days is defined as snow. Similarly, in the descending order of Julian days from D^{s}_{max} to $D^{s}_{a,}$ the cloud pixel of the previous days (t − 1… t − n) is defined as 'no snow' if the pixel has 'no snow' on the day t. In both cases, we followed backward processing; that is, the image of the day t − 1 was first processed based on the image of day t, and then the image of the day t − 2 was processed based on the corrected image of t − 1 and so on.
(c) In the time series of a snow cycle from D^{s}_{a} to D^{s}_{max}, if the pixel has 'snow' cover on the day 't', and cloud in following days (t + 1,… t + n), the cloud pixel of the following days was assigned as 'snow'. While, in the time series of Julian day from D^{s}_{max} to D^{s}_{min} of the given snow cycle, the cloud pixel in the following days (t + 1… t + n) is assigned as 'no snow', if the pixel has 'no snow' cover on the day t. In both cases, we followed forward processing.

The missing data day was treated as 100% cloud cover and was filled, based on the temporal position of the day in a snow cycle, and the above-mentioned decision rules (a to c).

3.3. Accuracy assessment of cloud removal methodology

Since no ground station snow data is available in the region, we followed the Gafurov and Bárdossy (2009) procedure. This procedure is based on the comparison of original MODIS snow-cover data with least cloud cover as a 'ground truth' data against cloud-generated MODIS snow-cover data as an 'observed', to evaluate the performance of the proposed methodology. At first, we randomly selected ten MODIS snow cover data which met two criteria: a) that have least cloud cover (<5%); and b) the cloud cover differences between two satellite data in that day is at least 40% (Table 2). The 40% threshold for cloud-cover difference between the two satellites was used, since the implementation of the first step alone could remove the most of the cloud of 'observed data' (cloud-filled data used in the validation process) if the difference between the two satellite images is very low.

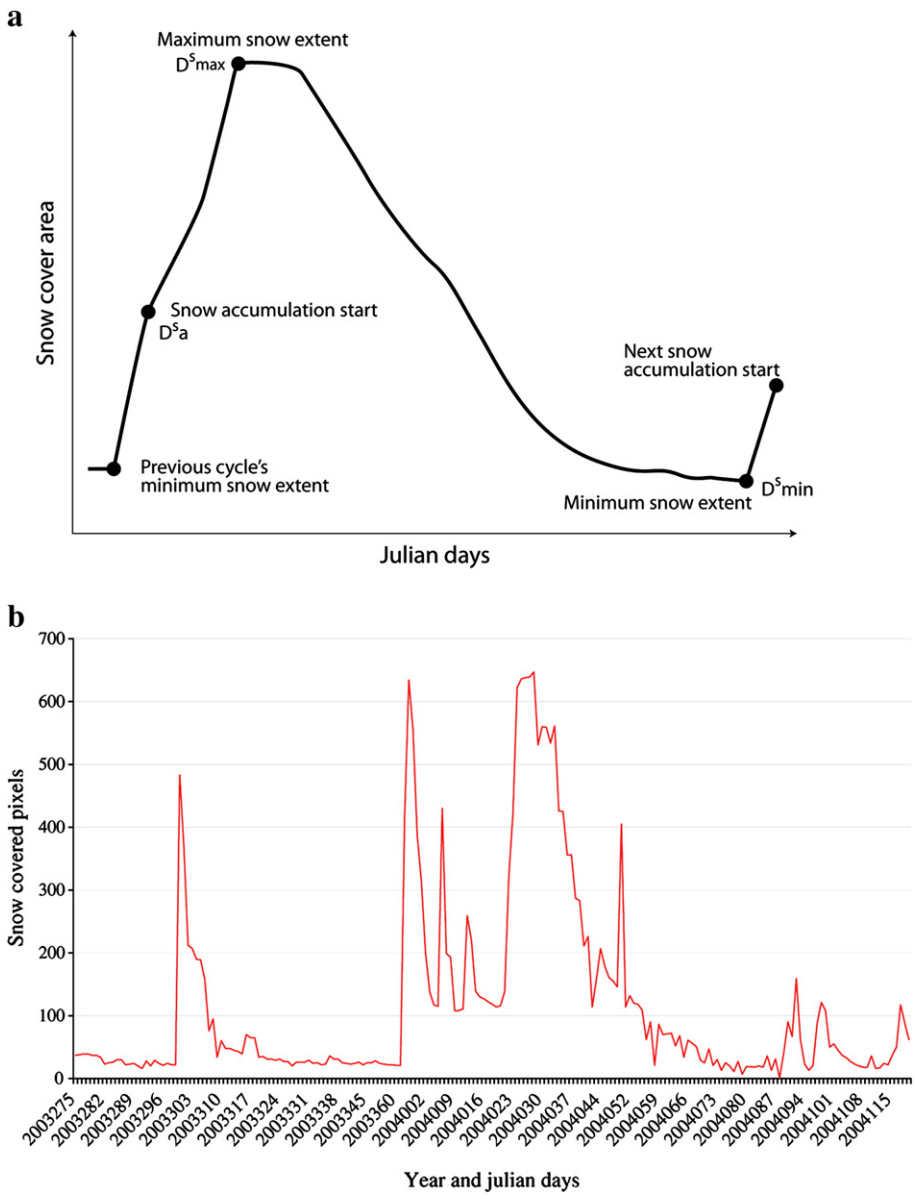

Fig. 3. Snow cycle: a) an ideal snow cycle; b) snow-cover pattern (showing many snow cycles) after step 4 in a zone located in upper Mustang in the snow season 2003/04.

The selected images were then filled by clouds of another dense cloud-cover product. The dense cloud-cover products, used to fill clouds in the selected least cloud-covered images, were also randomly selected from other years than the 'ground truth' image. The resulting snow-cover data with assigned cloud-cover pixels were used as input ('observed' image) for proposed methodology, and their respective original images were used as the 'ground truth' data. The resulting 'observed' images have cloud cover greater than 70% (Table 2). Since for the period 2000–2002, when only Terra data was available and the original Terra data was used directly as input for the second step, the validation of proposed methodology was done in two parts : with all steps; and excluding the first step to examine the effect of the first step.

The agreement of the resulting classification from the proposed method was calculated by comparing it with the original images. A confusion matrix, which measures agreement in classification and misclassification (underestimation error — classify snow as no snow; and overestimation error — classify no snow cover as snow) (Gao et al., 2010; Parajka & Blöschl, 2008), was used to estimate the accuracy of the proposed methodology. The overall degree of agreement (O_A), underestimation error (E_U) and overestimation error (E_O) was calculated as (all in percentages):

$$O_A = \frac{C_s^s + C_{ns}^{ns}}{T_c} \times 100 \tag{7}$$

$$E_U = \frac{C_{ns}^{s}}{T_c} \times 100 \tag{8}$$

$$E_O = \frac{C_s^{ns}}{T_c} \times 100 \tag{9}$$

where, C_s^s and C_{ns}^{ns} are the sum of pixels correctly classified as snow and no snow cover respectively from cloud (in the filled image); C_{ns}^{s} is the sum of the snow pixels incorrectly classified as no snow; C_s^{ns} is the sum of no snow pixels incorrectly classified as snow, and T_c is the total number of cloud pixels in the filled image.

Table 2
Images used for validation process.

Original Terra (used as ground truth for validation)		Cloud cover filled by (Terra image)	Cloud cover % after cloud assigned (used as observed data for validation)	Cloud % in Aqua image
Image date	Cloud cover (%)			
13 Mar 2004	2.57	30 Jan 2008	89.42	53.34
22 Nov 2004	3.29	18 Feb 2002	70.31	67.73
19 Dec 2004	3.14	7 Nov 2002	79.65	94.70
21 Mar 2005	1.24	26 Jan 2004	84.99	81.98
12 Mar 2006	4.93	17 Jan 2008	83.62	64.60
30 Mar 2006	3.84	28 Apr 2003	71.84	58.09
5 Jan 2007	3.95	20 Feb 2001	81.20	54.77
12 Dec 2009	5.0	15 Apr 2001	84.36	66.50
7 Feb 2010	4.56	15 Mar 2002	76.32	73.85
27 Mar 2010	1.58	5 Mar 2001	86.35	51.63

3.4. Spatial and temporal variability assessment

In order to examine the variability and trend of snow-cover duration in the study area, we computed anomalies of maximum snow-cover extent, simple statistical measure 'coefficient of variance' for each month of the snow season and an annual linear trend per pixel. The significance of trend was evaluated using the Student's *t* test.

4. Results

4.1. Effectiveness of cloud removal methodology

The five-step cloud removal method applied in this study produced almost cloud-free daily images, leaving only 1.82% cloud cover on average, where the highest cloud remaining was 3.91%. On average, the combination of Terra and Aqua products, the adjacent temporal deduction, a spatial filter based on orthogonal neighbouring pixels, zonal snowline and snow cycle methods, respectively, reduced cloud cover by 21.03, 12.69, 1.02, 38.28 and 25.16% in the last 10 years' snow season data. Depending on the relative spatial and temporal position of cloud-cover pixels, with reference to non-cloud pixels, different steps perform differently for each day's image (Fig. 4a). Monthly average snow-cover percentages after implementation of each step are presented in Fig. 4b. The combination of Terra and Aqua performed well when the cloud-cover pattern in both products was different. Similarly, the temporal deduction approach, based on one day forward and one day backward images' information, performed well when both previous and the next day images were cloud-free or had relatively low cloud coverage. The performance of the zonal snowline method was better when there was cloud cover at very high and very low elevations, and the respective zone had a low cloud-cover percentage. Theoretically, the zonal snow cycle method largely depends upon the precise identification of the snow cycle for the given zone. Its performance is highly influenced by the relative temporal position of the cloud pixel in the snow cycle. During backward processing (rule 'b' in Section 3.2.5), the performance was better if the days closer to the end of snow cycle were cloud-free. However, during the forward processing (rule 'c' in Section 3.2.5), the cloud removal performance was better if the days at the beginning of the snow cycle had relatively low cloud cover. Fig. 5 shows an example of cloud fraction removed after each step for 20 February, 2005.

The validation test, based on a comparison of the results of the cloud removal methods applied in 'cloud-filled images' with respective original images, shows the successful and efficient performance of the proposed methodology (five steps), as more than 99% of cloud was removed with a disagreement error of less than 8% (Tables 3 and 4), while the implementation of the second to fifth steps, excluding the first step, can remove 98.83% of cloud, with a disagreement error of less than 9%. As expected, the inclusion of the first step removes more cloud with low disagreement error. However, the difference in total cloud elimination and error percentage is not so high between including and excluding the first step. Moreover, excluding the first step performs better with a low level of error, with higher cloud cover removal on two validation test days: 13 March, 2004, and 12 March, 2006 (Table 4). Hence, the use of Terra data directly as the input in the second step for the period 2000–2002 — when Aqua data was not available, which could result in low cloud removal (i.e. 0.41% less) and

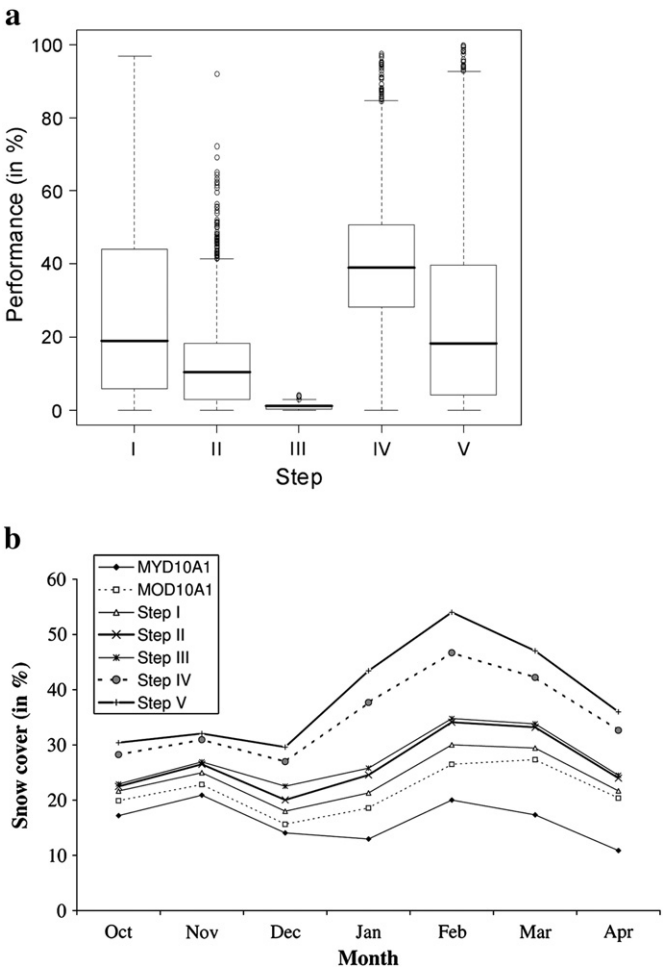

Fig. 4. Performance of five subsequent steps when applied together: a) performance to remove cloud (in %); b) mean percentage (monthly) snow coverage of the Terra MODIS (MOD10A1), Aqua MODIS (MYD10A1) and after implementation of step I, step II, step III, step IV and step V; the distance between two successive steps' line graph shows the increase mean monthly snow cover % at higher order step. The results are means of the entire study area during 2000–2010.

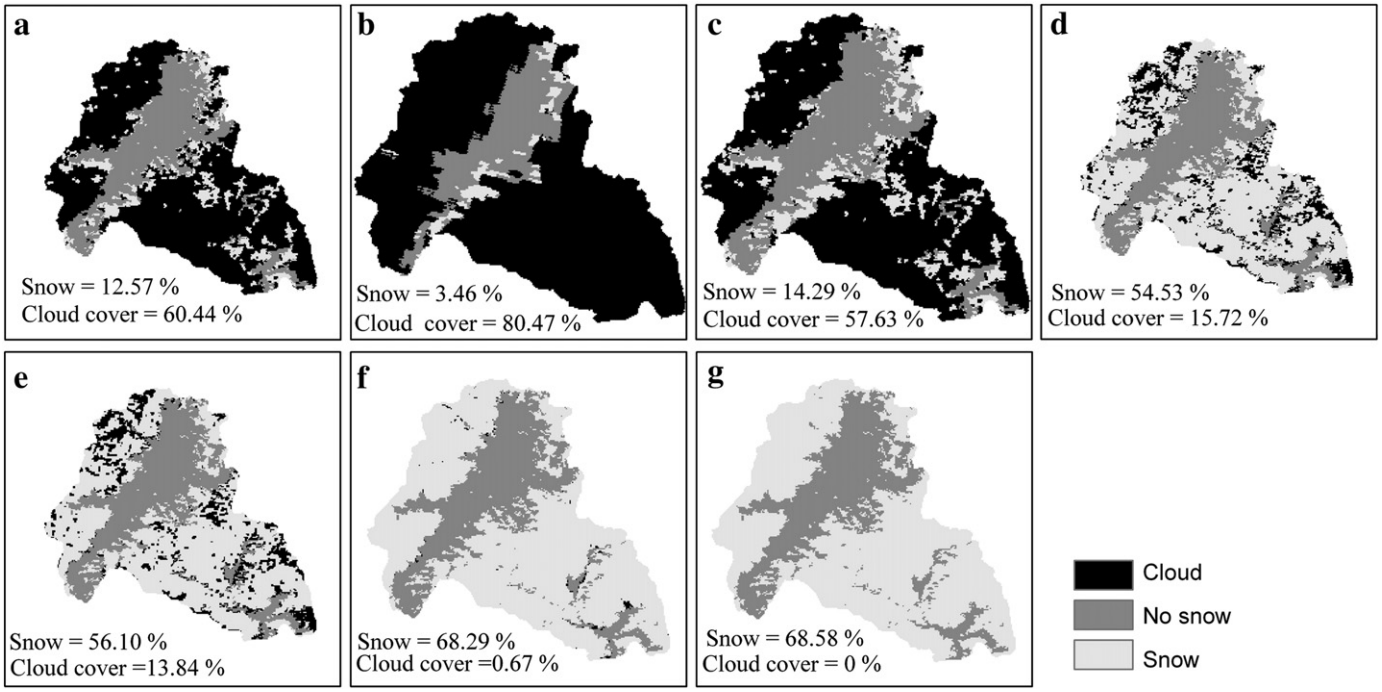

Fig. 5. Cloud cover of original MODIS images and after implementation of five steps for 20 Feb, 2005: a) original MODIS Aqua; b) Original MODIS Terra; and c–e) after implementation of successive steps (I–V).

slightly higher disagreement error (1.25%) — do not significantly affect the result.

4.2. Spatial temporal variability of snow cover

Although average annual snow cover percentage in the last decade shows a declining pattern (0.53%yr^{-1}), the significance test shows that the trend is not statistically different from zero. However, the time series of snow-cover anomalies shows very high interannual and intra-seasonal variability (Figs. 6 and 7). For instance, the average annual snow cover in the region during the snow season of 2005/06 was about 50%, while in 2008/09 it was only 29%. One of the striking features observed in the region was the significant delay of the maximum snow extent day in the snow season ($R^2 = 0.52$, $p = 0.019$), with an annual delay of 6.7 days yr^{-1} (Fig. 7). The maximum snow extent day in a year in the snow season represents the peak snowfall/

Table 3
Validation result for each step (in %).

Steps	With all steps (step I to V)					Excluding step I				
	Total cloud elimination	Agreement	Disagreement			Total cloud elimination	TRUE	Disagreement		
			OE	UE	Total			OE	UE	Total
Step 1	48.31	45.84	0.80	1.66	2.47					
Step 2	9.27	8.71	0.35	0.21	0.56	41.51	40.50	0.59	0.42	1.01
Step 3	0.70	0.63	0.03	0.03	0.07	0.60	0.54	0.04	0.02	0.06
Step 4	12.62	11.19	0.87	0.56	1.43	15.50	13.52	1.74	0.24	1.98
Step 5	28.34	25.37	1.95	1.01	2.97	41.22	35.54	3.60	2.08	5.68
Total	99.24	91.75	4.02	3.47	7.49	98.83	90.09	5.96	2.77	8.74

Table 4
Validation result for different days (in %).

Test date	With all steps					Excluding step 1				
	Total cloud elimination	TRUE	Disagreement error			Total cloud elimination	TRUE	Disagreement error		
			UE	OE	Total			UE	OE	Total
13 Mar 2004	99.09	89.30	6.97	2.82	9.79	99.02	90.70	4.49	3.83	8.32
22 Nov 2004	99.24	91.49	3.81	3.94	7.75	96.15	87.43	1.94	6.78	8.72
19 Dec 2004	99.53	93.95	2.91	2.68	5.58	99.37	87.66	2.03	9.68	11.71
21 Mar 2005	99.78	90.81	3.78	5.19	8.97	99.69	87.56	5.99	6.15	12.14
12 Mar 2006	99.42	96.23	2.85	0.33	3.18	99.85	97.31	2.18	0.37	2.54
30 Mar 2006	98.50	88.72	3.70	6.08	9.78	98.63	86.07	1.35	11.22	12.56
5 Jan 2007	99.68	93.50	2.32	3.85	6.17	98.78	92.15	0.65	5.98	6.63
12 Dec 2009	99.47	92.30	1.70	5.48	7.17	97.01	90.40	1.64	4.96	6.60
7 Feb 2010	99.12	91.82	1.93	5.37	7.30	99.93	91.82	0.97	7.14	8.11
27 Mar 2010	98.59	89.40	4.76	4.43	9.19	99.89	89.84	6.53	3.52	10.05
Average	99.24	91.75	3.47	4.02	7.49	98.83	90.09	2.77	5.96	8.74

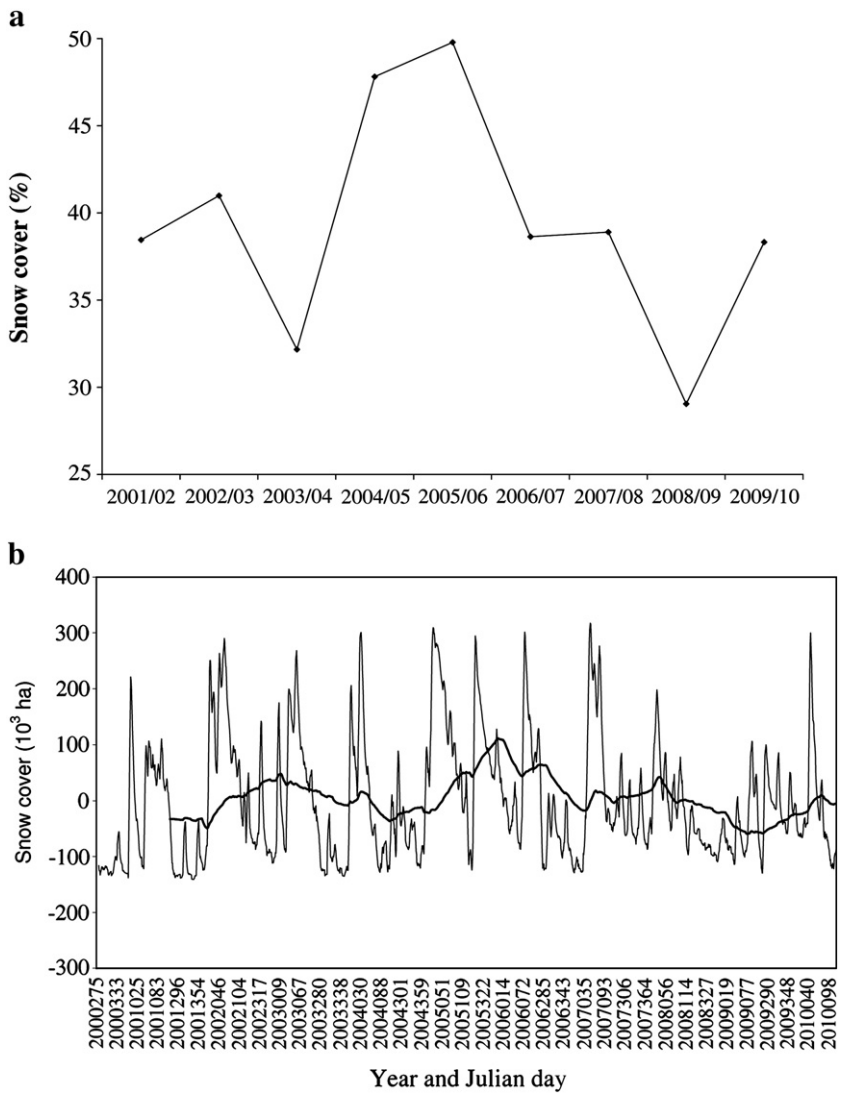

Fig. 6. Snow-cover variability during last decade: a) average snow cover; b) snow-cover anomalies.

accumulation of the year. Comparing the peak snow accumulation days, the average peak snow accumulation in the first half of the decade occurred around the second week of January, while in the second half of the decade it occurred around the end of February. Similarly, the second half of the decade was also characterized by a continuous decline in average snow cover. It confirms the shift in the snow season and the recent decline in snow as frequently perceived by the local people.[1] In terms of average snow cover and maximum snow extent, 2008/09 was found to be the most snow-poor hydrological season in the last decade. The minimum snow cover day during the snow season, that represents the peak snowmelt period in the year, occurred between 20 and 27 April in 2003/04, 2007/08, 2008/09 and 2009/10, while in the remaining years it occurred within second week of October. The occurrence of the minimum snow extent day in October (at the beginning of snow season) in these years indicates the late snowmelt, that is in May or in the summer months. However, in order to draw a definitive conclusion about the shifting pattern of the minimum snow extent day or the complete snowmelt in the study region, the data for the whole year needs to be analysed.

[1] First author conducted three group discussions and semi to unstructured interviews with 74 persons during March to May 2009 about their experience and perception of climate change and snow cover dynamics.

The comparison of average snow cover by month revealed that not only was the peak snow time delayed, but also the maximum snow-covered month (having the highest average snow cover in the snow season) shifted forward by about one month. Consequently, Feb/March appeared as the snow months compared to Dec/Jan, which are considered as the ideal snow months in the region, and local agropastoral activities (calendar) have been structured accordingly. Within the last decade, March has had the highest average snow cover in 2000/01, 2005/06, 2006/07 and 2008/09. Similarly, February has had the highest average snow cover in the remaining years except 2003/04. Contrary to the general perception, December has lower average snow cover than April, as portrayed by the line graph of the monthly average snow-cover percentages after step five in Fig. 4b. The early and late snow was the main reason behind this.

Long-term (2000/01 to 2009/10) average snow-cover duration in the snow season ranges from about 5 days, on the valley floor of Lower Mustang in the south, to 213 days in the high-altitude, perennial snow-cover area. As expected, annual average snow-cover duration was found to be strongly correlated with elevation ($r = 0.83$, $p < 0.0001$). Fig. 8 shows the spatial distribution of average seasonal snow-cover duration. Similar to the annual average, seasonal average snow-cover duration was also found to correlate strongly with elevation, with $r > 0.8$ in all three observed months of post-monsoon, winter and pre-monsoon seasons. Most of the northern and central

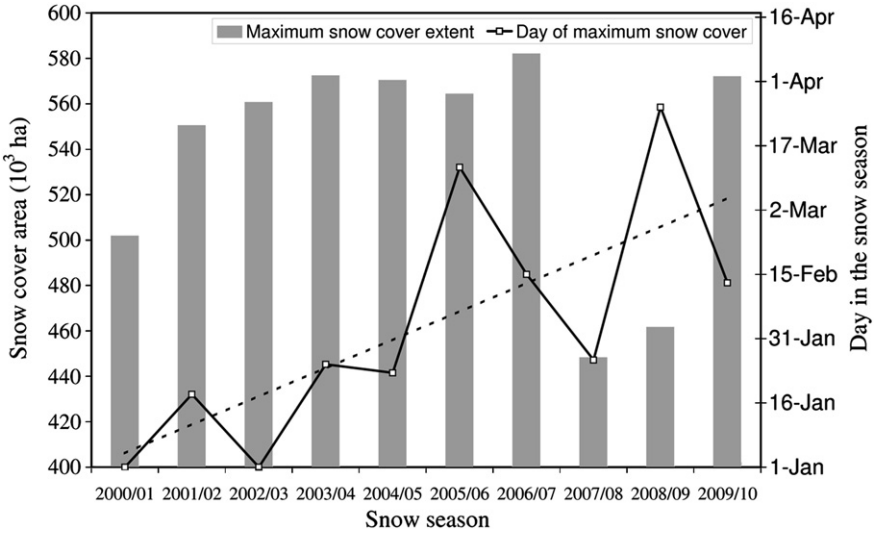

Fig. 7. Maximum snow-cover extent and day of maximum snow cover (peak snow).

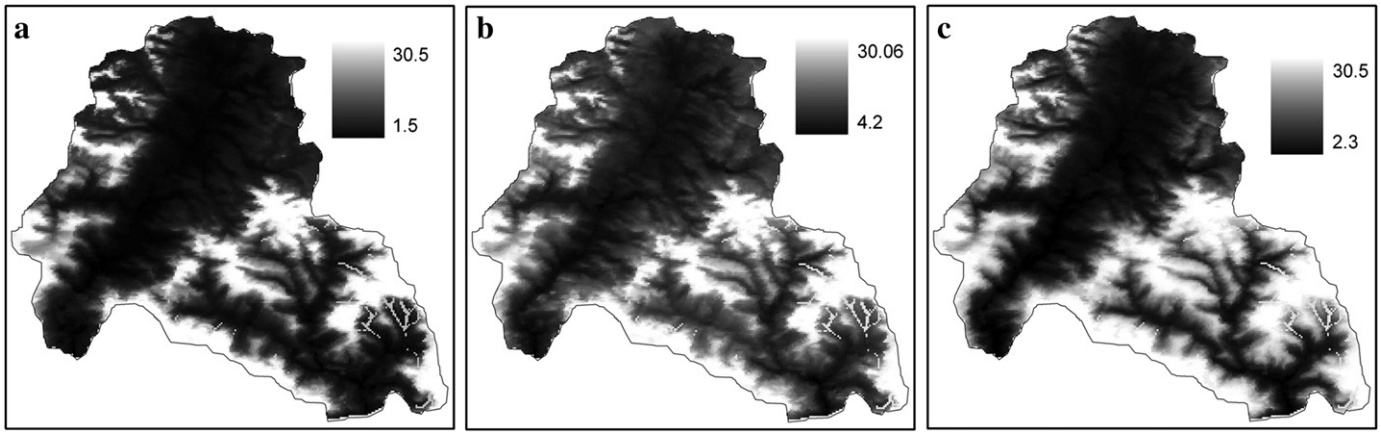

Fig. 8. Seasonal average snow-cover duration (in days:) a) post-monsoon (Oct/Nov); b) winter (Dec/Feb); c) pre-monsoon (March/Apr).

areas of Mustang district, mainly rangeland areas, are affected by the most substantial year-to-year fluctuation in snow-cover duration, with the coefficient of variation (COV) greater than 50% (Fig. 9). In addition, narrow patches of rangeland and cultivated land along the valley floor in Lower Mustang and the Nar-Phu Valley also have the highest fluctuation of annual snow-cover duration, with COV greater than 50%. About 62% of the area has COV greater than 30%. In general, the coefficient is highest in the regions with the least snow cover. All winter months have a similar spatial pattern of interannual variability of average monthly snow cover. The striking analogy between Fig. 9a and b suggests a similar spatial pattern of monthly and annual variability of snow-cover duration, although there is a difference in coefficient. At this point it would be worth mentioning another notable feature; that the area with the largest coefficient of variability

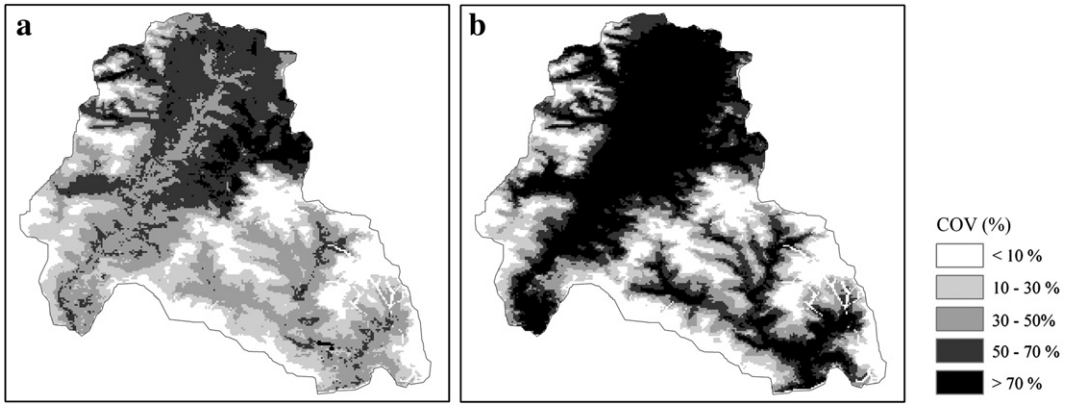

Fig. 9. Variability maps for: a) annual snow cover days; and b) monthly snow-cover days of April (The maps shows coefficient of variability (COV)).

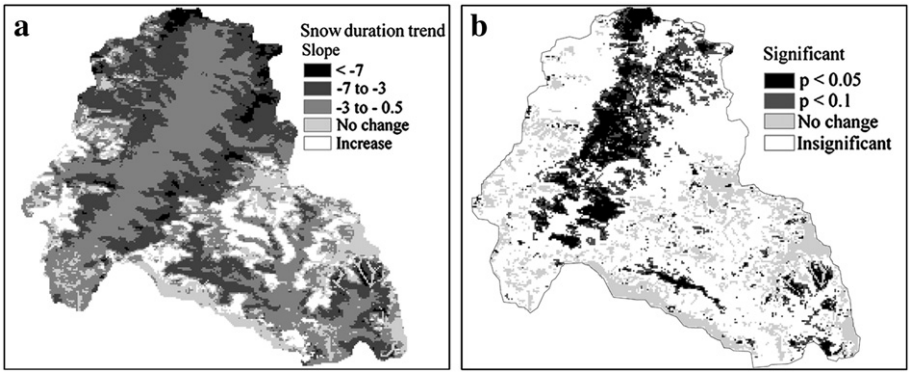

Fig. 10. Snow-cover duration trend from 2001/02 to 2009/10: a) trend; and b) significance of trend. Trends are termed insignificant for pixels in which $p<0.1$.

is highest in the early snow season months and higher in the snowmelt season (mainly April) compared to peak snow months.

A pixel-wise linear trend analysis of annual snow-cover duration shows that about 77.6% of the area of the Manang and Mustang districts has a declining trend (Fig. 10a). However, only 14.15% pixels with a declining trend are statistically significant, with $p<0.05$, and the next 14.2% of the area with a negative trend in annual snow cover during 2001/02 to 2009/10 is significant, with $p<0.1$ (Fig. 10b). Most of these pixels are located in the arid to semi-arid rangeland and the cultivated lands of Upper Mustang, and the cultivated land and valley floor of Upper Manang. About 11.2% of pixels exhibit no or very marginal changes (i.e. slope<0.5 days per year), which were considered stable. All these pixels are located at high altitude and most of them represent the permanent snow cover area. Although 11.1% of pixels have an increasing trend in annual snow cover days, a significance test shows they are not statistically different from zero.

5. Discussion and conclusion

The five successive steps approach proposed in the study, to estimate the pixel cover for cloud observed areas, was based on spatial and temporal filtering, using time series MODIS images, topographic features, such as elevation, slope and aspect and land cover map for the data-limited region of the Nepalese THR. The purpose of the sequenced order of steps is to increase the efficiency of each step and minimize the error. The efficiency of the fifth step largely depends upon the precise identification of snow cycles, snow accumulation start, and maximum and minimum snow extent days of a cycle in a given zone. This depends upon the proportion of cloud in the given zone. A higher proportion of cloud free pixels in the given zone can lead to the precise identification of the snow cycle and consequent low level of error. That is why it is placed last so that input to this step could have a low cloud proportion. As stated earlier, the performance of the zonal snowline approach also depends upon the amount of cloud-free pixels in a zone. However, it makes an inference only when there is 25% cloud-free pixel. That is why this step is placed fourth, earlier than the zonal snow cycle approach. In the temporal combination, the proposed order of steps maintains the increasing temporal window, from a few hours to snow cycles, so that associated uncertainty in each step can be minimized. The first step combines the information from two different satellites of the same day with a few hours of time shift. The second step combines the information from adjacent days while the fifth step combines the information from the time window of a snow cycle. The Terra and Aqua images are not only acquired at different times, but also their snow mapping algorithm is different, since the Terra snow-mapping algorithm uses MODIS band 6 instead of band 7, as used to produce MYD10A1 (Riggs et al., 2006). Consequently, the combination of Terra and Aqua products also produces little disagreement owing to the change in snow accumulation or melt during the shifting time on that day (Gafurov & Bárdossy, 2009), or owing to a misclassification error as a result to a change in algorithm under some conditions (Parajka & Blöschl, 2008). Gao et al. (2010) found a higher snow underestimation error in both Terra and Aqua snow-cover images than overestimation error. So, we used a prioritization scheme of snow, no snow and cloud in combination. However, we admit that this step is biased toward 'snow'. The high range of performance of the first step to remove the cloud cover (Fig. 4a) reflects the fact that the clouds were in continuous dynamic movement.

The second step uses the information of the previous and the next day's images to deduce the surface condition (snow or no snow) of cloud pixels on the current day image, assuming similar conditions in a cloud pixel of the current day if both the preceding and the following images have the same cover type (snow or no snow). Similar to what other researchers have found, the adjacent temporal deduction approach performed very well, removing an additional 12.69% of cloud cover with low disagreement errors (cf. Gafurov & Bárdossy, 2009; Gao et al., 2010). However, in the situation of daily changes in snow cover this assumption may bear some limitations. Although the spatial filter based on orthogonal neighbouring pixels relatively lower cloud cover percentage, it also has a very low disagreement error which is why we also considered it as the part of the methodology, as Gafurov and Bárdossy (2009) did.

It is well known that the topographical factors and land cover influence the snow accumulation and ablation pattern (cf. Meiman, 1970), and the strong radiation in this region makes these factors even more important. Not only does the spatial pattern of snowmelt rates vary with differences in incoming radiation, as a function of aspect, elevation and slope, but also accumulation varies according to the sweeping and deposition of snow by wind (Akyürek & Orman, 2002; Dunn & Colohan, 1999; Fitzharris, 1978; Male & Gray, 1981; Meiman, 1970). The regional snowline method of Parajka et al. (2010) and the snow transition elevation step of Gafurov and Bárdossy (2009) incorporated the influence of elevation on snow accumulation and ablation behaviour to remove cloud pixels. However, their approaches still ignore the influence of aspect, slope and land cover. The zonal snow transition line approach (the fourth step in this study) attempted to incorporate the influence of topographic factors (aspect and slope) and land cover in the spatial variability of snow accumulation and ablation during the deduction process. The performance, removing 38.28% additional cloud cover, and the validation test (having less than 2% misclassification error) indicates that this step is efficient to remove the cloud coverage.

Gafurov and Bárdossy's (2009) approach, which considers the 'first snow covered day' and 'first snowmelt day' as the threshold days of snow accumulation start and melt cannot capture the reality, and leads to more misclassification errors since there could be many snow cycles in a zone within a snow season, as shown in Fig. 3b. The zonal snow cycle approach used in this study works well and presents a good alternative where there are many snow cycles within a year. The

validation test shows this step only has a 2.97% disagreement error, which clearly indicates its higher accuracy compared to that of Gafurov and Bárdossy (2009).

Using the proposed methodology it was possible to eliminate more than 98% of cloud coverage and monitor snow-cover dynamics with very low disagreement error figures. Overall, our results demonstrate that the five steps approach used in this study presents a robust technique, which can not only reduce the cloud coverage, but also gives good agreement measures.

The results indicate the high interannual maximum snow cover extent, high interannual and intra-seasonal variability of average snow cover, and snow-cover duration. The shift forward in the annual maximum snow extent day by about 6.7 days per year, and the highest average snow cover to Feb/March, indicates the delay in peak snowfall period, as well as a shift in main snow months. The oral history also confirms the high variability and shift in snow periods and months in the region. A substantial decline in snow-cover duration in the last decade was found in arid to semi-arid rangeland and cultivated land. These are areas where the wind effect is very high. A longer time series of data, however, needs to be examined to reach a definitive conclusion about temporal trends. Similarly, a very high (>50%) coefficient of variability in annual snow-cover duration was found in the major agropastoral production areas (rangeland and arable land). Such a decline and high variability of snow-cover duration in agropastoral production areas could have a significant impact on local agropastoral production and livelihood.

Acknowledgements

Thanks to the Norwegian State Education Loan Fund (Lånekassen) for funding the first author. We especially thank three anonymous reviewers and the editor for critical review, valuable comments and suggestions that greatly helped to improve the manuscript.

References

Akyürek, Z., & Orman, A. (2002). Monitoring snow-covered areas using NOAA-AVHRR data in the eastern part of Turkey/Suivi des zones enneigées dans l'Est de la Turquie grâce à des données NOAA-AVHRR. *Hydrological Sciences Journal*, *47*(2), 243−252.

Baral, D. J., & Gupta, R. P. (1997). Integration of satellite sensor data with DEM for the study of snow cover distribution and depletion pattern. *International Journal of Remote Sensing*, *18*(18), 3889−3894.

Barnes, W. L., Pagano, T. S., & Salomonson, V. V. (2002). Prelaunch characteristics of the moderate resolution imaging spectroradiometer (MODIS) on EOS-AM1. *IEEE Transactions on Geoscience and Remote Sensing*, *36*(4), 1088−1100.

Barnett, T. P., Dümenil, L., Schlese, U., Roeckner, E., & Latif, M. (1989). The effect of Eurasian snow cover on regional and global climate variations. *Journal of Atmospheric Sciences*, *46*(5), 661−686.

Bates, B., Kundzewicz, Z. W., Wu, S., & Palutikof, J. P. (2008). *Climate change and water. Technical Paper of the Intergovernmental Pannel on Climate Change.* Geneva: IPCC Secretariat.

Berry, M. O. (1981). Snow and climate. *Handbook of Snow: Principles, Processes, Management and Use* (pp. 32−59).

Cruz, R. V., Harasawa, H., Lal, M., Wu, S., Anokhin, Y., Punsalmaa, B., et al. (2007). Asia. Climate change 2007: Impacts, adaptation and vulnerability. In M. L. Parry, O. F. Canziani, J. P. Palutikof, P. J. van der Linden, & C. E. Hanson (Eds.), *Contribution of Working Group II to the Fourth Assessment Report of the Intergovernmental Panel on Climate Change* (pp. 469−506). Cambridge: Cambridge University Press.

Dunn, S. M., & Colohan, R. J. E. (1999). Developing the snow component of a distributed hydrological model: A step-wise approach based on multi-objective analysis. *Journal of Hydrology*, *223*(1–2), 1−16.

Dyurgerov, M. B., Meier, M. F., & University of Colorado, B. I. o. A., & Alpine, R. (2005). *Glaciers and the changing Earth system: A 2004 snapshot.* University of Colorado Boulder: Institute of Arctic and Alpine Research.

Erikson, M., Xu, J., Bhakta Shrestha, A., Ananda Vaidy, R., Nepal, S., & Sandström, K. (2009). *The changing Himalayas—Impact of climate change on water resources and livelihoods in the Greater Himalayas.* Kathmandu: International Centre for Integrated Mountain Development.

Fitzharris, B. B. (1978). Problems in estimating snow accumulation with elevation on New Zealand mountains. *Journal of Hydrology. New Zealand*, *17*(2), 78−90.

Gafurov, A., & Bárdossy, A. (2009). Cloud removal methodology from MODIS snow cover product. *Hydrology and Earth System Sciences*, *13*, 1361−1373.

Gao, Y., Xie, H., Yao, T., & Xue, C. (2010). Integrated assessment on multi-temporal and multi-sensor combinations for reducing cloud obscuration of MODIS snow cover products of the Pacific Northwest USA. *Remote Sensing of Environment*, *114*, 1662−1675.

Guenther, B., Xiong, X., Salomonson, V. V., Barnes, W. L., & Young, J. (2002). On-orbit performance of the Earth Observing System Moderate Resolution Imaging Spectroradiometer: First year of data. *Remote Sensing of Environment*, *83*(1–2), 16−30.

Guglielmin, M., Aldighieri, B., & Testa, B. (2003). PERMACLIM: A model for the distribution of mountain permafrost, based on climatic observations. *Geomorphology*, *51*(4), 245−257.

Hall, D. K., Foster, J. L., Verbyla, D. L., Klein, A. G., & Benson, C. S. (1998). Assessment of snow-cover mapping accuracy in a variety of vegetation-cover densities in central Alaska. *Remote Sensing of Environment*, *66*(2), 129−137.

Hall, D. K., & Riggs, G. A. (2007). Accuracy assessment of the MODIS snow products. *Hydrological Processes*, *21*(12), 1534−1547.

Hall, D. K., Riggs, G. A., & Salomonson, V. V. (1995). Development of methods for mapping global snow cover using moderate resolution imaging spectroradiometer data. *Remote Sensing of Environment*, *54*(2), 127−140.

Hall, D. K., Riggs, G. A., & Salomonson, V. V. (2001). Algorithm theoretical basis document (ATBD) for the MODIS snow and sea ice-mapping algorithms. 53 pp. Available online at. http://modis-snow-ice.gsfc.nasa.gov/atbd01.html.

Hall, D. K., Riggs, G. A., Salomonson, V. V., DiGirolamo, N. E., & Bayr, K. J. (2002). MODIS snow-cover products. *Remote Sensing of Environment*, *83*(1–2), 181−194.

Lemke, P., Ren, J., Alley, R. B., Allison, I., Carrasco, J., Flato, G., et al. (2007). Observations: Changes in snow, ice and frozen ground. *Climate change*, 337−383.

Liang, T. G., Huang, X. D., Wu, C. X., Liu, X. Y., Li, W. L., Guo, Z. G., et al. (2008). An application of MODIS data to snow cover monitoring in a pastoral area: A case study in Northern Xinjiang, China. *Remote Sensing of Environment*, *112*(4), 1514−1526.

Liu, X., & Chen, B. (2000). Climatic warming in the Tibetan Plateau during recent decades. *International Journal of Climatology*, *20*(14), 1729−1742.

Male, D. H., & Gray, D. M. (1981). Snowcover ablation and runoff. *Handbook of snow—Principles, processes, management & use* (pp. 360−436).

Maurer, E. P., Rhoads, J. D., Dubayah, R. O., & Lettenmaier, D. P. (2003). Evaluation of the snow-covered area data product from MODIS. *Hydrological Processes*, *17*(1), 59−71.

Meiman, J. R. (1970). Snow accumulation related to elevation, aspect and forest canopy. *Snow Hydrology*, 35−47.

Messerli, B., Viviroli, D., & Weingartner, R. (2004). Mountains of the world: Vulnerable water towers for the 21st Century. *Ambio*, 29−34.

Mitchell, K. M., & DeWalle, D. R. (1998). Application of the snowmelt runoff model using multiple parameter landscape zones on the Towanda Creek Basin, Pennsylvania. *Journal of the American Water Resources*, *34*(2), 335−346.

MODIS Reprojection Tool (MRT) (2008). *User's manual, release 4.0* (pp. 62). Available from https://lpdaac.usgs.gov/lpdaac/content/.../MRT_Users_Manual.pdf.

Parajka, J., & Blöschl, G. (2006). Validation of MODIS snow cover images over Austria. *Hydrology and Earth System Sciences Discussions*, *3*, 1569−1601.

Parajka, J., & Blöschl, G. (2008). Spatio-temporal combination of MODIS images—Potential for snow cover mapping. *Water Resources Research*, *44*(3), W03406.

Parajka, J., Pepe, M., Rampini, A., Rossi, S., & Blöschl, G. (2010). A regional snow-line method for estimating snow cover from MODIS during cloud cover. *Journal of Hydrology*, *381*, 203−212.

Paudel, K. P. (2006). Institutions, environmental entitlements and pastoral management: A case of Nyishang, Trans-Himalaya region, Manang District, Nepal Unpublished M. Phil. thesis, University of Bergen, Norway.

Paudel, K. P., & Andersen, P. (2010). Assessing rangeland degradation using multi temporal satellite images and grazing pressure surface model in Upper Mustang, Trans Himalaya, Nepal. *Remote Sensing of Environment*, *114*(8), 1845−1855.

Riggs, G. A., Hall, D. K., & Salomonson, V. V. (2006). MODIS snow products user guide to collection 5. Available from. http://modis-snow-ice.gsfc.nasa.gov/sug_c5.pdf

Robinson, D. A., Dewey, K. F., & Heim, R. R. (1993). Global snow cover monitoring: An update. *Bulletin of the American Meteorological Society*, *74*, 1689.

Robock, A. (1980). The seasonal cycle of snow cover, sea ice and surface albedo. *Monthly Weather Review*, *108*(3), 267−285.

Salomonson, V. V., & Appel, I. (2004). Estimating fractional snow cover from MODIS using the normalized difference snow index. *Remote Sensing of Environment*, *89*(3), 351−360.

Seyfried, M. S., & Wilcox, B. P. (1995). Scale and the nature of spatial variability: Field examples having implications for hydrologic modeling. *Water Resources Research*, *31*(1), 173−184.

Shrestha, A. B., Wake, C. P., Mayewski, P. A., & Dibb, J. E. (1999). Maximum temperature trends in the Himalaya and its vicinity: An analysis based on temperature records from Nepal for the period 1971–94. *Journal of Climate*, *12*(9), 2775−2786.

Singh, P., & Bengtsson, L. (2005). Impact of warmer climate on melt and evaporation for the rainfed, snowfed and glacierfed basins in the Himalayan region. *Journal of Hydrology*, *300*(1–4), 140−154.

Solomon, S., Qin, D., Manning, M., Chen, Z., Marquis, M., Averyt, K. B., et al. (2007). *Climate change 2007: The physical science basis.* Cambridge and New York: Cambridge University Press.

Tekeli, A. E., Akyürek, Z., Arda Sorman, A., Sensoy, A., & Ünal Sorman, A. (2005). Using MODIS snow cover maps in modeling snowmelt runoff process in the eastern part of Turkey. *Remote Sensing of Environment*, *97*(2), 216−230.

Tong, J., Déry, S. J., & Jackson, P. L. (2009). Topographic control of snow distribution in an alpine watershed of western Canada inferred from spatially-filtered MODIS snow products. *Hydrology and Earth System Sciences*, *13*(3), 319−326.

Wang, X., Xie, H., & Liang, T. (2008). Evaluation of MODIS snow cover and cloud mask and its application in Northern Xinjiang, China. *Remote Sensing of Environment*, *112*(4), 1497−1513.

Wang, X., Xie, H., Liang, T., & Huang, X. (2009). Comparison and validation of MODIS standard and new combination of Terra and Aqua snow cover products in northern Xinjiang, China. *Hydrological Processes*, *23*(3), 419−429.

Xie, H., Wang, X., & Liang, T. (2009). Development and assessment of combined Terra and Aqua snow cover products in Colorado Plateau, USA and northern Xinjiang, China. *Journal of Applied Remote Sensing*, *3*(033559), 033559.

Xu, J., Grumbine, R., Shrestha, A., Eriksson, M., Yang, X., Wang, Y., et al. (2009). The melting Himalayas: Cascading effects of climate change on water, biodiversity, and livelihoods. *Conservation Biology*, *23*(3), 520−530.

Zhao, H., & Fernandes, R. (2009). Daily snow cover estimation from Advanced Very High Resolution Radiometer Polar Pathfinder data over Northern Hemisphere land surfaces during 1982–2004. *Journal of Geophysical Research*, *114*(D5).

Zhou, X., Xie, H., & Hendrickx, J. M. H. (2005). Statistical evaluation of remotely sensed snow-cover products with constraints from streamflow and SNOTEL measurements. *Remote Sensing of Environment*, *94*(2), 214−231.